Adsorption of pyridine from aqueous solutions by polymeric adsorbents MN 200 and MN 500. Part 1: Adsorption performance and PFG-NMR studies

Qingyu Zhu, Geoff D. Moggridge*, Mohamed Ainte, Mick D. Mantle, Lynn F. Gladden, Carmine D'Agostino*

***Corresponding authors:**

Dr Carmine D'Agostino

Address: Department of Chemical Engineering and Biotechnology, University of Cambridge, Pembroke Street, Cambridge, CB2 3RA, UK

Email: cd419@cam.ac.uk

Telephone: +44 (0)1223 761628

Fax: +44 (0)1223 334796

Dr Geoff Moggridge

Address: Department of Chemical Engineering and Biotechnology, University of Cambridge, Pembroke Street, Cambridge, CB2 3RA, UK

Email: gdm14@cam.ac.uk

Telephone: +44 (0)1223 334763

Fax: +44 (0)1223 334796

Abstract

The removal of pyridine from aqueous solutions was carried out using Macronet polymeric adsorbents MN 200 and MN 500. The optimal pyridine uptakes were in approximately neutral solutions as a result of optimal effect of π -π hydrophobic and attractive electrostatic interactions between pyridine and the adsorbents. These adsorbents showed superior pyridine uptake capacities than some apatite and activated carbons in isotherm studies. Thermodynamic analysis showed that pyridine adsorption is exothermic on MN 200 and endothermic on MN 500, implying that the adsorption on MN 500 is an activated process, which is attributed to the presence of sulfonic acid groups. Pseudo-first and second order rate models were used to fit the adsorption kinetics for the adsorbents. Translational dynamics of guest molecules within the porous polymers was analysed by PFG-NMR diffusion technique and the diffusion behaviour was characterised by two distinctive diffusion regions. PFG-NMR derived self-diffusion coefficients of pyridine in MN 500 were much slower than the expected diffusion coefficients based on a purely geometrical confinement effect, which suggests the interaction of pyridine with the sulfonic acid groups on MN 500 and their stronger effect on diffusivity also enhances the adsorption performance of this adsorbent. These studies reveal new insights into adsorption properties of pyridine in porous polymers in relation to the structural and surface properties probed by PFG-NMR and account for the effectiveness of these adsorbents in the treatment of waste water containing the aromatic N-heterocyclic compound.

Key words: Pyridine removal, Macronet adsorbents, PFG-NMR, adsorption isotherms, thermodynamics, kinetics

1. Introduction

Aromatic N-heterocyclic compounds are reported to exhibit a wide range of toxicity among various life forms [1]. There are significant amounts of aromatic N-heterocyclic compounds as effluents released into the environment as a result of industrial activities associated with coal and shale oil processing, and pharmaceuticals, pesticides, dyes, and food additive production [2]. These aromatic N-heterocyclic compounds are present at lower concentrations but more soluble than their homocyclic analogues, and therefore can be easily transported through soil and contaminated ground water [2], leading to increased bioavailability and thus potential toxic effects. Pyridine is a basic N-heterocyclic organic compound. Due to its wide range of applications, pyridine has been detected in both surface and ground water, showing toxicity to aquatic life and creating nuisance [3]. Therefore, pyridine removal is of great importance to prevent or minimise damages to health and environment.

To remediate the wastewater, adsorption over highly porous materials has attracted much attention because of its high efficiency and lower energy consumption. One major advantage lies in the fact that persistent compounds are removed, rather than being broken down to potentially dangerous metabolites such as those produced by oxidative or reductive processes [2]. The most commonly used adsorbent is activated carbon prepared from various waste materials [4–7], though activated carbon may suffer the drawback of low mechanical strength which makes regeneration for re-use difficult and cost-intensive [8]. Alternative sorbents such as polymeric resins have been frequently used in wastewater treatment to overcome this problem [9–11]. More recently, Macronet polymeric adsorbents have been developed and successfully applied for removal of both organic and inorganic impurities from water [12–14]. Macronet materials are chloromethylated polystyrene/divinylbenzene copolymers presenting a hypercrosslinked structure that provides controlled pore sizes and relatively high surface areas. These materials possess both macro- and micro-porosity at the same time, which is that are retained from their swollen-state in synthesis

[15]. The performance can be further enhanced by using the increased polarity obtainable by the presence on the adsorbent's internal surface of a minor amount of polar functional groups [16].

In this work, the significance of Macronet hypercrosslinked polymeric adsorbents will be reported for pyridine removal from aqueous solutions in batch experiments, by evaluating the adsorption performance in terms of adsorption isotherms, thermodynamic and kinetic properties. In addition, the adsorption performance inside the polymeric matrix and its relation with adsorbents' structural and surface properties will be established for the first time by analysing the translational dynamics of the guest molecules from their diffusion properties in the pore space using the pulsed-field gradient (PFG)-NMR diffusion technique.

2. Materials and methods

2.1. Materials

Pyridine (99.8%) was purchased from Sigma Aldrich. Macronet adsorbents MN 200 and MN 500 were provided by Purolite Ltd. The adsorbents were carefully washed with deionised water and acetone, and dried at 60 ^{0}C for 24 hours before use. The dried adsorbents were sieved and those of diameter in the range 0.55-0.75 mm were used to minimise particle size variation in affecting the experiment performance.

2.2. Self-diffusion measurements

NMR diffusion experiments were carried out with a Bruker DMX 300 spectrometer operating at a frequency of 300.13 MHz equipped with a diffusion probe capable of producing magnetic field gradient pulses up to 11.76 T/m in the z-direction. A Bruker Variable Temperature unit, BVT 3000, was used to set the required temperature 20 ^{0}C for each experiment. Prior to loading into the

magnet bore, the polymer samples were prepared by soaking the polymer beads in the liquids for at least 24 h to equilibrate. They were then dried on a pre-soaked filter paper to remove any excess liquid on the external surface and finally placed in a 5 mm NMR tube. To minimise errors due to evaporation of volatile liquids, adsorbent filter paper with a small amount of pure liquid was placed under the cap of the NMR tubes, which was sealed using parafilm. Both the liquid and polymer samples were left for approximately 20 min at 20 ^{0}C to reach thermal equilibrium before starting the NMR experiment.

Self-diffusion coefficients were measured using the pulsed gradient stimulated echo (PGSTE) pulse sequence [17] for the bulk liquids and the alternating pulsed-field gradient stimulated echo (APGSTE) [18] for liquids inside the porous polymers, in order to minimise the effect of any background gradient associated with differences in magnetic susceptibility for liquids in the porous materials. In general, the attenuation of the NMR signal, (E) is related to the experimental variables and the self-diffusion coefficient in each region (D) according to:

$$E = \exp\left[-D\gamma^2 g^2 \delta^2 \left(\Delta - \frac{\delta}{3}\right)\right] \quad (1)$$

where γ is the gyromagnetic ratio of the nuclei (^{1}H) being studied, g is the strength of the gradient pulse of duration δ, and Δ is the time interval between the leading edges of the gradient pulses (set to 50 ms). Measurements were performed by holding δ constant and varying g in a number of up to 16 increments.

2.3. Adsorption equilibrium and kinetics

Experiments to study adsorption equilibrium and kinetics were conducted in a batch reactor. A weighed sample of the sorbent (63 mg) was poured into 150 mg/L pyridine aqueous solution, which was stirred in a temperature-controlled flask equipped with a magnetic stirrer at a constant

temperature. Preliminary tests on adjusting the stirring speed from 200 to 600 rpm showed no marked change in kinetic profiles. Hence, to ensure complete mixing and to minimise external diffusion resistance, a stirring speed of 600 rpm was chosen for all the following experiments. .

The isotherm experiments were conducted with a series of 50-400 mg/L pyridine solutions from 25-55 ^{0}C for a time to reach adsorption equilibrium (24 h), after which 1.0 ml aliquots of the liquid phase were taken to determine the equilibrium concentrations. To obtain the adsorption kinetic profiles, aliquots of the solution were taken at certain time intervals from the moment the experiment started.

A Shimazu 160A UV-vis spectrophotometer was used to analyse the pyridine concentrations. Certain liquid aliquots were diluted to fit the calibration plot that was constructed in the pyridine concentration of 10-50 mg/L. The equilibrium pyridine uptake per unit mass of the sorbents (q_e) was determined as:

$$q_e = \frac{V(C_0 - C_e)}{m_s} \quad (2)$$

where C_0 and C_e are the initial and equilibrium concentrations of pyridine in solution, V is the solution volume and m_s is the adsorbent mass. The pyridine uptake (q) as a function of time t was determined similarly using Equation 2 by replacing the equilibrium pyridine concentration with the pyridine concentration at that time (C_t). The volume change of the solution by taking aliquots each time was taken into account to determine the pyridine uptake accurately. Each experiment was conducted for at least three times to have repeatable results.

3. Results and discussion

3.1. Adsorbent properties

The properties of the Macronet adsorbents MN 200 and MN 500 are well documented in the literature [8,13,19–21]. A summary of the properties is presented in Table 1. Due to the

functionalisation with the sulfonic acid groups that partially block the pores, MN 500 exhibits lower surface area compared to MN 200. Both materials present a hybrid pore structure possessing a considerable proportion of micropores, which originates from the post-crosslinking chloromethylated polystyrene/divinylbenzene formed in the polymerisation process [22]. There is a decrease in percentage of micropores from MN 200 to MN 500, which has also been shown in the pore size distribution analysis [23], indicating that sulfonation may significantly occur in the micropores. The sulfonic acid concentration in MN 500 is 3.1 mmol/g determined by sodium ion exchange [23], which makes MN 500more acidic and hydrophilic relative to MN 200.

Table 1. Properties of Macronet polymeric adsorbents MN 200 and MN 500.

Properties	MN 200	MN 500
BET surface area (m^2/g)	793	414
Micropore volume (cm^3/g)	0.25	0.14
Micropore (%)	68	48
Total pore volume (cm^3/g)	0.37	0.28
Average pore diameter (nm)	3.7	2.7
Average bead diameter (μm)	500-700	600
Solid phase density (g/m^3)	1150	1318[a]
Porosity (%)	59	27[a]
Functionality	none	$-SO_3H$
Reference	[13]	[8]

a: The solid phase density and porosity were elsewhere reported 1570 g/m^3 and 51 %, respectively. [19], which is more consistent with the results from [20].

3.2. Effect of solution pH on the adsorption performance

Pyridine adsorption uptake on MN 200 and MN 500 was studied by varying the initial solution pH from 4.3 to 10.3 with the initial pyridine concentration of 150 mg/L at 25 ^{0}C in the batch reactor. The initial solution pH was achieved by adding appropriate amount of HCl or NaOH solutions. Small changes of the solution pH were observed with the decline of pyridine concentration during the course of adsorption, which was considered negligible because the intervals of the chosen initial pH values are much larger (see Figure 1).

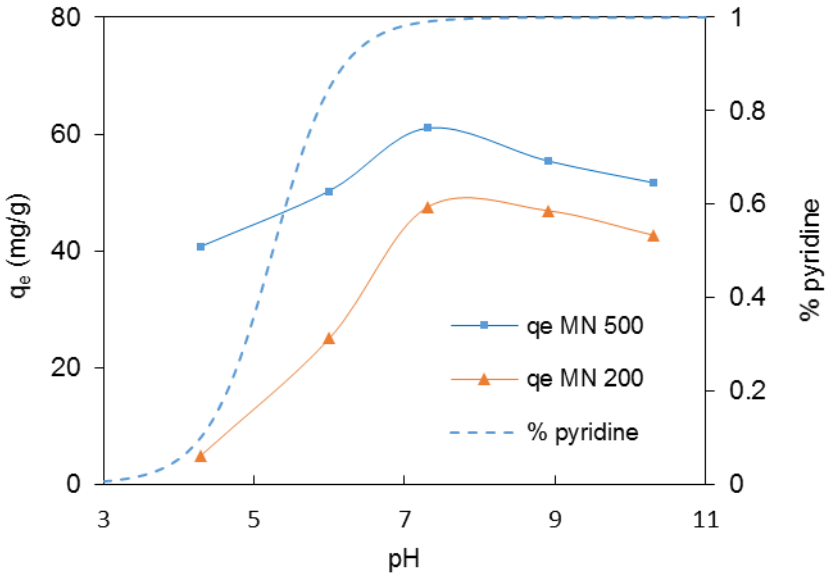

Figure 1. pH dependence of equilibrium adsorption uptake of pyridine onto MN 200 and MN 500 with the initial pyridine concentration of 150 mg/L at 25 ^{0}C. The relative error is approximately $\pm$ 10%.

The pyridine uptake on MN 200 and MN 500 and pyridine percentage as a function of initial solution pH are shown in Figure 1. Pyridine is expected to be protonated in acidic aqueous solutions to form positively charged pyridinium ions (pK_a 5.2) [24]. The percentage of non-protonated pyridine, depending on the solution pH, can be given by:

$$\% \text{ pyridine} = \frac{10^{pH-pKa}}{1+10^{pH-pKa}} \times 100 \quad (3)$$

It is clearly seen from the figure that the pyridine uptake increases with the increase of pH, reaching the maximum at nearly neutral solutions and starts decreasing as the pH increases further. Since the majority of the adsorbent surface is hydrophobic due to the polystyrene/divinylbenzene networks, pyridine adsorption on MN 200 and MN 500 is likely to be governed by the hydrophobic π-π interaction between pyridine and the adsorbent surfaces. With the protonation of the nitrogen atom in pyridine in acidic solutions, the π-π interaction for adsorption can be partly disrupted due to delocalisation of the positive charges on the aromatic structure in pyridine; hence the adsorption uptake is decreased [25].

In basic solutions, the pyridine uptake is lower compared to the maximal uptake in nearly neutral solutions for both adsorbents. This is because both adsorbents are more negatively charged and thus the attractive electrostatic interactions with pyridine molecules become weaker when the solution pH increases, though this finding is slightly different from what observed on activated carbon, where the adsorption amount remained approximately constant at pH over 7 [26].

Pyridine uptake on MN 200 reduces more markedly than on MN 500 when the solution is acidic. According to the pH titration curves, MN 200 and MN 500 exhibit points of zero charge (pH_{pzc}) of approximately 5.0-6.2 and 2.2, respectively [23]. This means as long as the solution pH is greater than 2.2, the MN 500 surface is mostly negatively charged and pyridine adsorption is favoured in acidic solutions due to attractive electrostatic interactions between the protonated pyridine and the negatively charged MN 500 surface. Conversely, because the pH_{pzc} of MN 200 (5.0-6.2) is similar to the pK_a of pyridine (5.2), at solution pH lower than this, both pyridine and MN 200 surface are mostly positively charged, generating repulsive electrostatic forces that can reduce pyridine adsorption favoured by π-π interaction [6]. The highest pyridine uptakes on both adsorbents were at the initial solution pH of 7.3, which is a compromise between effective π-π and electrostatic

interactions. Therefore, the optimal condition at a solution pH of 7.3 was used for further experiments.

3.3. Adsorption isotherms

The adsorption equilibrium is established when the quantity of the adsorbate in the bulk solution is in a dynamic balance with that adsorbed at the sorbent interface, and can be described by an adsorption isotherm model characterised by certain constants that represent the surface properties and the adsorbent-adsorbate affinity [27]. To find this relation, adsorption isotherms of pyridine adsorption on MN 200 and MN 500 from aqueous solutions were analysed at 25, 35, 45, 55 ^{0}C applying the Langmuir and Freundlich models.

The Langmuir model is one of the most commonly used isotherm models for describing removal of chemicals from aqueous solutions [27]. It assumes uniform energies of adsorption and that the maximum adsorption capacity corresponds to a saturated monolayer of solute molecules on the adsorbent surface:

$$q_e = \frac{q_m K_L C_e}{1+K_L C_e} \quad (4)$$

where q_e and C_e are the amount of solute adsorbed per unit weight of adsorbent and equilibrium concentration of pyridine in bulk solution, respectively, q_m is the maximum adsorption capacity, and K_L is the equilibrium constant related to the affinity of adsorption.

The model parameters were estimated with a nonlinear regression method where the sum of the squares of the errors was minimised with the optimisation algorithm of Rosenbrock-Newton [26,28]:

$$Minimum = \sum(y_e - y_c)^2 \quad (5)$$

where y_e and y_c are the experimental and calculated values. The quality of the non-linear fitting of each model was evaluated using the average relative deviation in percentage (ARD):

$$ARD\ (\%) = \frac{1}{n}\sum \left|\frac{y_e - y_c}{y_e}\right| \times 100 \quad (6)$$

where n is the number of samples and the variable y represents the equilibrium uptake of pyridine on the adsorbents (q_e).

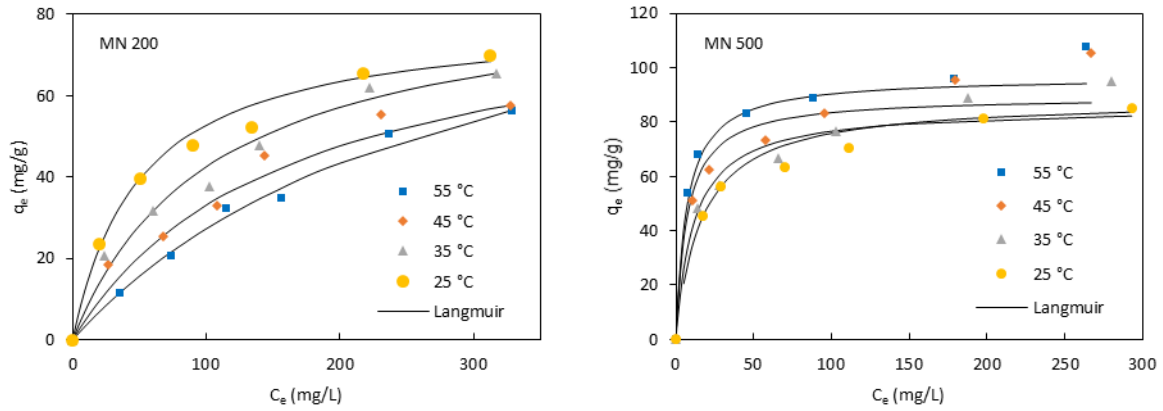

Figure 2. Adsorption isotherms of pyridine from aqueous solutions on MN 200 and MN 500 fitted to the Langmuir model. The uncertainty on the experimental values of pyridine uptake is approximately $\pm$10 %.

Adsorption isotherms of pyridine on MN 200 and MN 500 at different temperatures were fitted to the Langmuir model and are presented in Figure 2. Fittings to the Freundlich model are shown in Supplementary Information. It can be clearly seen that pyridine uptake on MN 200 decreases while that on MN 500 increases with the increasing temperature, which indicates the exothermic and endothermic nature of adsorption on MN 200 and MN 500, respectively. According to the Langmuir and Freundlich parameters, along with average relative deviation (ARD) values given in Table 2, no

significant difference suggests the preference of one isotherm model to the other, though it can be seen that the Freundlich model might better describe pyridine adsorption on MN 500.

Table 2. Parameters of the Langmuir and Freundlich models for the adsorption of pyridine on MN 200 and MN 500 and the average relative deviations (ARD) between the modelled and experimental equilibrium pyridine uptakes. The method for estimating errors in the calculated parameters is shown in the Supplementary Information.

Isotherm model	Parameter							
	MN 200				MN 500			
T (^{0}C)	25	35	45	55	25	35	45	55
Langmuir								
q_m (mg/g)	81.1±4.0	87.3±7.3	85.6±12.5	105±13.7	88.4±4.4	85.5±6.4	89.5±7.4	96.0±4.5
K_L (10^{-2}L/mg)	1.90±0.30	0.95±0.20	0.63±0.20	0.35±0.07	6.4±1.5	8.6±3.6	14.0±7.4	17.3±4.9
ARD (%)	4.3	6.8	8.6	4.0	5.2	7.0	6.9	4.5
Freundlich								
α	2.37±0.21	2.16±0.25	1.97±0.31	1.35±0.14	4.20±0.58	4.34±0.18	4.55±0.37	5.20±0.63
K_F ($mg^{1-1/\alpha}L^{1/\alpha}/g$)	6.60±1.26	4.72±1.34	3.10±1.33	0.83±0.35	22.0±3.57	26.5±1.19	30.6±4.37	36.9±3.9
ARD (%)	4.9	3.6	7.4	7.7	2.7	1.4	1.4	3.9

One of the most important isotherm parameters to evaluate the performance of an adsorbent is the uptake capacity. Most reports in the literature concerning pyridine uptake capacity describe uptake performances in terms of the Langmuir maximum uptake values (q_m). It is noted that despite it does not always provide the best fit to the experimental data compared to the other isotherm models, the Langmuir isotherm still provides reasonably good fits and can be used to compare the adsorption performance with other materials reported in the literature, listed in Table 3. It is shown that the Macronet adsorbents MN 200 and MN 500 are superior in pyridine uptake in comparison with some activated carbons and apatite and are comparable to another hypercrosslinked fibre adsorbent.

Table 3. Comparison of adsorption capacities of various adsorbents for pyridine in aqueous solutions.

Adsorbent	q_m (mg/g)	T (^{0}C)	Reference
MN 200	81.1	25	This work
MN 500	86.0	25	This work
Hypercrosslinked fibre	142	15	[29]
Hypercrosslinked fibre	131	30	[29]
Commercial granular activated carbon	20.5	20	[6]
Activated carbon from rice husk ash	11.7	20	[6]
Apatite from phosphate rock	40.2	20	[24]
Microporous apatite from phosphate rock	46.8	20	[24]
Porous hydroapatite	42.5	20	[24]
Commercial activated carbon fabric cloth	53.7	25	[4]
Activated carbon from coconut fibres	40.5	25	[4]
Activated carbon from coconut shell	20.5	25	[4]
Activated carbon from acid treated coconut fibres	111	25	[4]
Activated carbon from acid treated coconut shell	50.1	25	[4]

3.4. Thermodynamic properties

Thermodynamic properties of the adsorption processes of pyridine from aqueous solutions on MN 200 and MN 500 were determined with the initial pyridine concentration of 150 mg/L in the temperature range of 25-55 ^{0}C. The change of Gibbs free energy (ΔG^0) was determined as:

$$\Delta G^0 = -RTlnK_a \tag{7}$$

where K_a is the equilibrium constant of adsorption, R is the gas constant and T is temperature. The enthalpy (ΔH^0) and entropy (ΔS^0) changes of adsorption can be obtained, respectively, from the gradient and the intercept of the linear plot of lnK_a versus $1/T$, assuming temperature independence of enthalpy and entropy changes in the small temperature range:

$$lnK_a = -\frac{\Delta H^0}{RT} + \frac{\Delta S^0}{R} \tag{8}$$

K_a is often determined from the ratio of equilibrium pyridine uptake on the adsorbent to the equilibrium concentration in bulk solution [30], or is treated equivalent to K_L or α, from the best-fit Langmuir or Freundlich models respectively [29,31]. All of the methods were found to result in similar ΔH^0 and ΔS^0 values for pyridine adsorption on both MN 200 and MN 500. Therefore, the thermodynamic parameters determined with K_a as the Langmuir constant (K_L) were reported for discussion, shown in Table 4.

The negative values of ΔG^0 indicate the feasibility and spontaneity of the adsorption processes. The negative value of ΔH^0 (-45.8 kJ/mol) for MN 200 confirms the exothermic nature of the process, which is consistent with pyridine adsorption reported on an in-house made hypercrosslinked fibre [29]. ΔS^0 for MN 200 is also negative, which is not rarely encountered for adsorption processes and is ascribed to an indication of no surface change upon adsorption [4]. Conversely, pyridine adsorption on MN 500 is endothermic, showing a positive enthalpy change. This implies that the adsorption on MN 500 is an activated process which may be due to the activation of sulfonic acid groups to favour their interaction with pyridine molecules. As the temperature increases, more acid sites are activated for adsorption, which increases randomness at the solid-solution interface, hence showing the positive ΔS^0.

Table 4. Thermodynamic parameters for adsorption of pyridine onto MN 200 and MN 500 from aqueous solutions. The method for estimating errors in the calculated parameters is shown in the Supplementary Information..

Adsorbent	T (^{0}C)	ΔG^0 (kJ/mol)	ΔH^0 (kJ/mol)	ΔS^0 (J/(mol K))
MN 200	25	-9.70±0.37	-45.8±3.1	-186±10.0
	35	-11.9±0.55		
	45	-13.4±0.87		
	55	-15.4±0.55		
MN 500	25	-6.95±0.63	29.7±2.7	76.3±8.6
	35	-6.29±1.14		
	45	-5.20±1.56		
	55	-4.79±0.79		

3.5. Adsorption kinetics

To describe the uptake of organic solutes onto solid sorbents, various adsorption kinetic mechanistic models have been used [32]. To obviate to the complexity, the simplest empirical expressions as analogy to those of reaction kinetics are preferred. The pseudo-first order kinetic model was used as follows [33]:

$$q = q_e\left(1 - e^{-k_1 t}\right) \tag{9}$$

where k_1 is the pseudo-first order rate constant for adsorption, the other symbols exhibit the same meanings as in Equation 2. The pseudo-second order equation is given by [34]:

$$q = \frac{q_e^2 k_2 t}{1 + q_e k_2 t} \tag{10}$$

where k_2 is the pseudo-second order rate constant for adsorption.

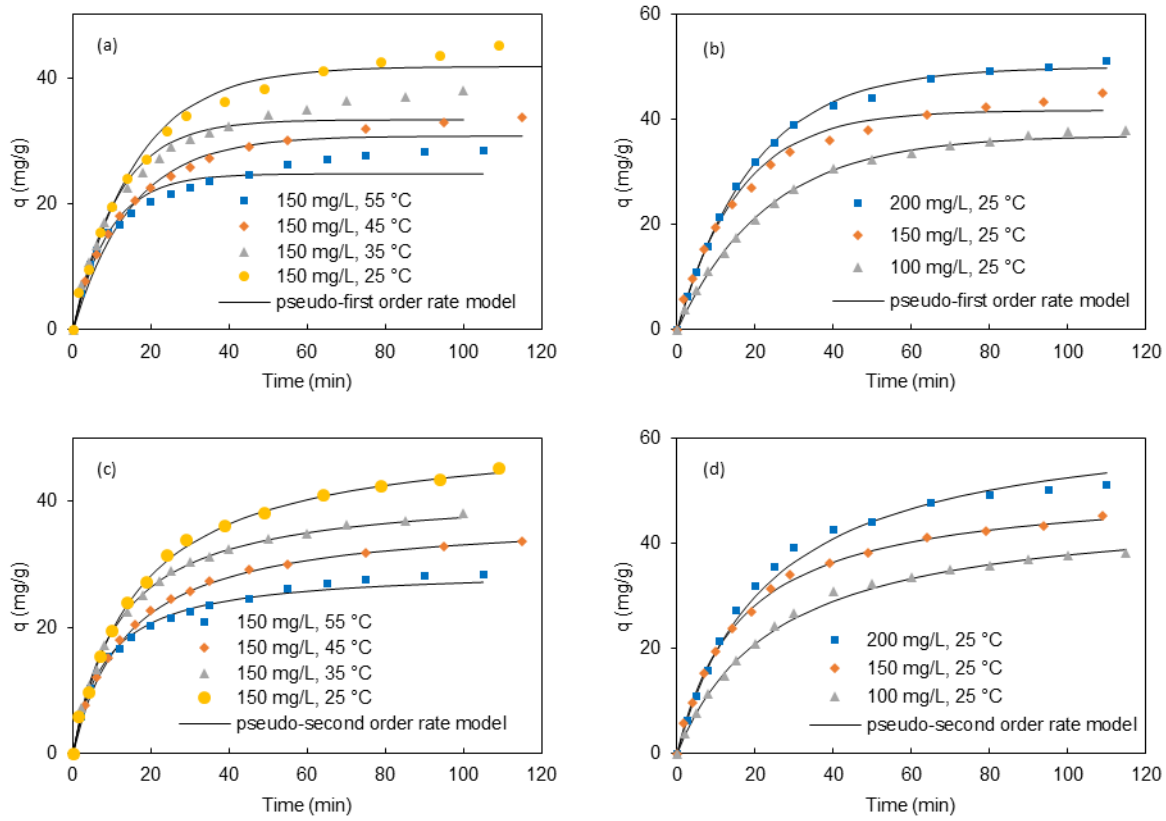

Figure 3. Pseudo-first and pseudo-second order rate models fitted to the kinetics of pyridine adsorption from aqueous solutions on MN 200 at various adsorption temperatures and initial pyridine concentrations. (a) and (c): at different temperatures with a fixed initial pyridine concentration of 150 mg/L; (b) and (d): at different initial pyridine concentrations with a fixed temperature of 25 ^{0}C. The uncertainty on experimental values of pyridine uptake is approximately $\pm$10 %.

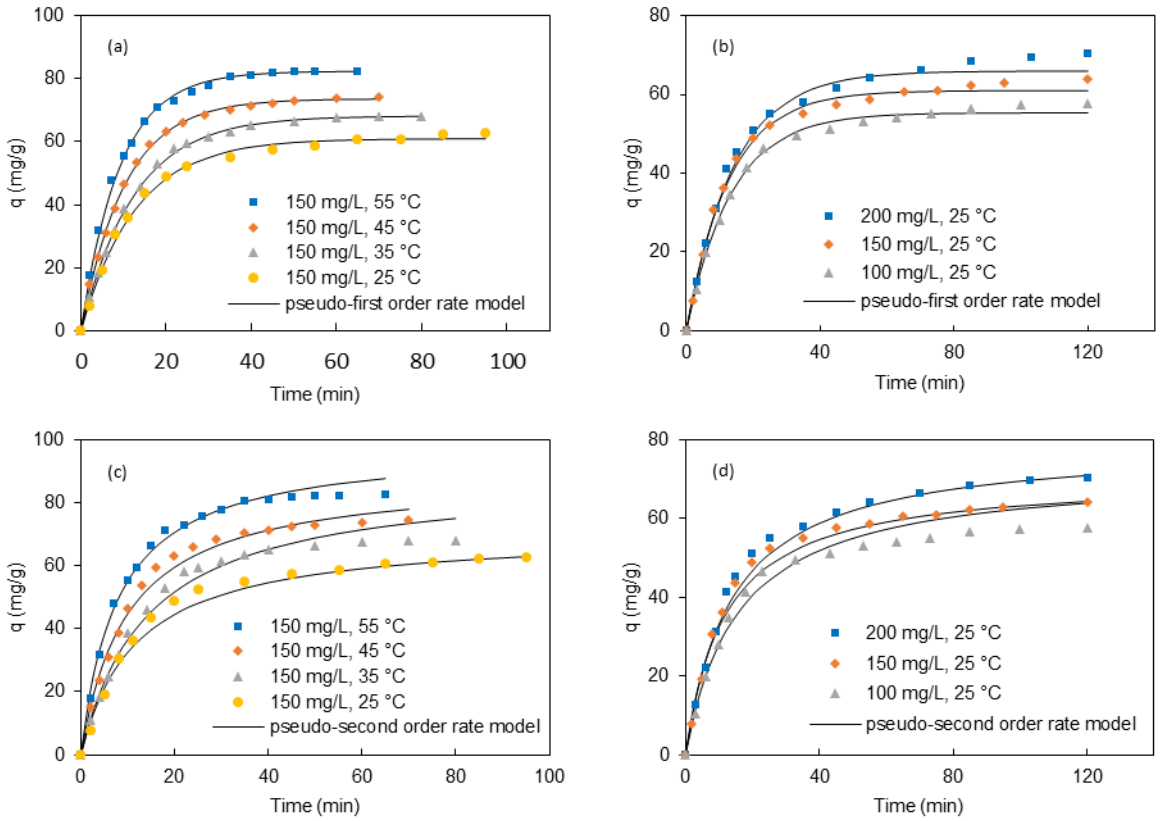

Figure 4. Pseudo-first and pseudo-second order rate models fitted to the kinetics of pyridine adsorption from aqueous solutions on MN 500 at various adsorption temperatures and initial pyridine concentrations. (a) and (c): at different temperatures with a fixed initial pyridine concentration of 150 mg/L; (b) and (d): at different initial pyridine concentrations with a fixed temperature of 25 ^{0}C. The uncertainty on experimental values of pyridine uptake is approximately $\pm$10 %.

Figures 3 and 4 show the experimental kinetic progresses of pyridine adsorption onto MN 200 and MN 500 fitted by pseudo-first and pseudo-second order models. The performance of each model was analysed by minimised ARD values with the optimised model parameters. The model parameters are summarised in Tables 5 and 6 along with the ARD values. Interestingly, as the initial pyridine concentration decreases, the best-fit rate model for pyridine adsorption on MN 200 shifts

from the pseudo-first to pseudo-second order, while the change of temperature does not cause the best-fit kinetic model to shift from one to the other. This implies that adsorption kinetics on MN 200 is limited by the number of adsorption sites and dependent on the initial pyridine concentration.

Table 5. Parameters of kinetic models for pyridine adsorption on MN 200 from aqueous solutions and average relative deviations (ARD) between model predictions and experimental kinetic data. Values of $q_{e\,expt}$ were taken as the equilibrium pyridine uptake at 24 hours. The method for estimating errors in the calculated parameters is shown in the Supplementary Information.

	parameters					
T (^{0}C)	25	25	25	35	45	55
C_0 (mg/L)	100	150	200	150	150	150
$q_{e\,expt}$ (mg/g)	40.6	47.6	53.2	40.3	34.2	29.1
Pseudo-first order						
k_1 (10^{-3}/s)	0.72±0.02	1.05±0.07	0.72±0.02	1.48±0.10	1.13±0.75	1.13±0.20
q_e (mg/g)	37.0±0.3	41.8±0.8	50.1±0.4	33.4±0.6	30.8±0.6	24.8±0.7
ARD (%)	2.9	5.5	1.8	4.9	5.7	7.0
Pseudo-second order						
k_2 (10^{-5} g/(mgs))	1.38±0.09	2.00±0.08	1.18±0.14	3.42±0.10	3.17±0.03	6.80±0.50
q_e (mg/g)	47.4±0.5	51.2±0.7	64.7±2.2	41.8±0.3	37.8±0.4	29.3±0.4
ARD (%)	2.4	3.1	3.7	1.9	2.2	2.5

Table 6. Parameters of kinetic models for pyridine adsorption on MN 500 from aqueous solutions and average relative deviations (ARD) between model predictions and experimental kinetic data. Values of $q_{e\ expt}$ were taken as the equilibrium pyridine uptake at 24 hours. The method for estimating errors in the calculated parameters is shown in the Supplementary Information.

	parameters					
T (^{0}C)	25	25	25	35	45	55
C_0 (mg/L)	100	150	200	150	150	150
$q_{e\ expt}$ (mg/g)	58.9	64.9	70.5	70.4	75.7	83.3
Pseudo-first order						
k_1 (10^{-3}/s)	1.23±0.05	1.30±0.04	1.18±0.06	1.33±0.02	1.60±0.03	1.82±0.05
q_e (mg/g)	55.4±0.6	61.0±0.5	65.9±0.9	68.1±0.3	73.6±0.4	82.4±0.6
ARD (%)	2.3	3.2	2.9	1.5	1.9	2.1
Pseudo-second order						
k_2 (10^{-5} g/(mgs))	1.46±0.22	2.01±0.25	1.52±0.15	1.33±0.18	1.90±0.19	2.16±0.19
q_e (mg/g)	72.3±1.6	70.3±2.8	79.1±1.7	88.3±3.0	88.9±2.0	98.3±1.7
ARD (%)	6.0	6.1	4.5	4.8	3.8	3.2

In general, the adsorption kinetics of pyridine on MN 200 is best-fitted by the pseudo-second order rate equation while that of pyridine on MN 500 is best-fitted by the pseudo-first order rate equation. It is therefore reasonable to assume different adsorption mechanisms of pyridine on MN 200 and MN 500. Due to highly acidic group content, protonation of pyridine molecules by bound acidic groups on MN 500 in forming the salt products may be considered as one of the main ways for pyridine fixation, , in addition to the hydrophobic π-π interaction. The pore size distribution analysis has shown that the pore volume reduction in MN 500 mainly occurs below the pore size of 2 nm in comparison with MN 200 [23], which indicates that the sulfonation takes place mainly in the micropores. Meanwhile, pyridine uptake on MN 500 is significantly higher and faster compared to that on MN 200. It is plausible there is some correlation between sulfonation and adsorption rate. If adsorption takes place progressively from the macropores to the micropores, the difference in the

trends of the kinetic plots for the two types of adsorbent may suggest that due to the strong interaction between pyridine and sulfonic acid groups, adsorption is enhanced in the micropores in MN 500 as the adsorption is closer to equilibrium.

3.6. PFG-NMR measurements

To further characterise the pore structure and obtain information on pore network connectivity as well as on molecular interactions of the adsorbate within the porous matrix of these Macronet adsorbents, the pulsed-field gradient (PFG)-NMR technique was used to measure self-diffusion coefficients of guest molecules within the pores of the adsorbents. A PFG interaction parameter (ξ) can be defined as the ratio of the self-diffusion coefficient of the bulk liquid (D_0) to the self-diffusion coefficient of the same liquid inside the pore space (D_i) [35,36]:

$$\xi = \frac{D_0}{D_i} \tag{11}$$

This ratio is affected by both geometrical characteristics of the porous matrix (*i.e.,* connectivity of the porous network) and molecular interactions within the pore space. Consequently, if the interaction between guest molecules and the porous material as well as inter-molecular interactions are minimal, the PFG interaction parameter may be considered to be a good estimate of tortuosity of the porous material (τ) [35,37–39]:

$$\tau = \frac{D_0}{D_i} \tag{12}$$

This was shown to be the case for porous oxides using liquid alkanes as the probing molecule, for which several conditions are verified: i) the guest molecule does not have chemical functionalities hence the influence of inter-molecular interactions as well as interactions with the solid walls of the pore are minimised; ii) the guest molecule is much smaller compared to the pore size of the material; iii) the porous geometry of the material does not change in contact with the guest

molecule [35]. Caution is required to apply this method to characterise the tortuosity of polymeric materials because they may be prone to swelling in contact with liquids. As for the Macronet adsorbents used in this work, rigid porosity was achieved from the swollen-state in the manufacturing process, showing little or no change when in contact with the permeating liquid [16]. For example, the swelling factor for MN 200 was reported to be 5% in contact with liquids [21]. It is plausible to assume little or negligible difference in the pore network connectivity change due to swelling in these materials, thus the PFG parameters calculated are assumed to be dependent on structural properties and molecular interactions within the pore space in their swollen state.

Pyridine and water, as well as two non-polar compounds, cyclohexane and n-octane, were used as the guest molecules for the PFG-NMR studies. Experiments performed on dry MN 200 and MN 500 showed no PFG-NMR signal decay; hence all the PFG-NMR signal decays can be safely attributed to the guest molecules diffusing within the pore structure of the polymers. Figure 5 shows the log attenuation plots for these molecules in MN 200 and MN 500. It is interesting to note that the diffusive behaviour of all liquids within MN 200 and MN 500 is non-linear showing the presence of two diffusion regimes.

The diffusion coefficients calculated by fitting the two linear portions of the curve and the values are reported in Table 7. D_1 indicates the diffusion associated with the fast decay of the plot (higher slope) whereas D_2 indicates the diffusion associated with the slow decay of the plot (lower slope). The presence of two distinctive diffusion regimes indicates the existence of macroscopic heterogeneities of the porous matrix [40]. Given the bimodal property of pore structures of the hypercrosslinked polymer adsorbents, which show larger macropores (ca 100 nm) and smaller micropores (ca 2 nm) [41,42], it is reasonable to assign the fast and slow diffusion coefficients to the macroporous and the microporous regions respectively. Such diffusion behaviour has previously been observed for highly porous activated carbon catalysts with bimodal pore size distribution [43]. According to our knowledge, there have only been studies looking at diffusion of small molecules, such as water and

hydrocarbons, in other polymeric materials such as cellulose gels [44], polyglycolide [45,46] and more rigid polymer structures [47], which reported values of diffusivity in the same range reported here. The closest comparison can be made with the work of Seland et al. [47], who studied diffusion of organic solvents in porous polystyrene and polyethylene particles. Their results also showed a non-linear behaviour of the PFG-NMR attenuation plots, particularly marked for polyethylene particles, with the observation of two-diffusion components, assigned to diffusion of guest molecules in large cavities (order of few μm) and the semi-crystalline areas of the polymer(order of nm).

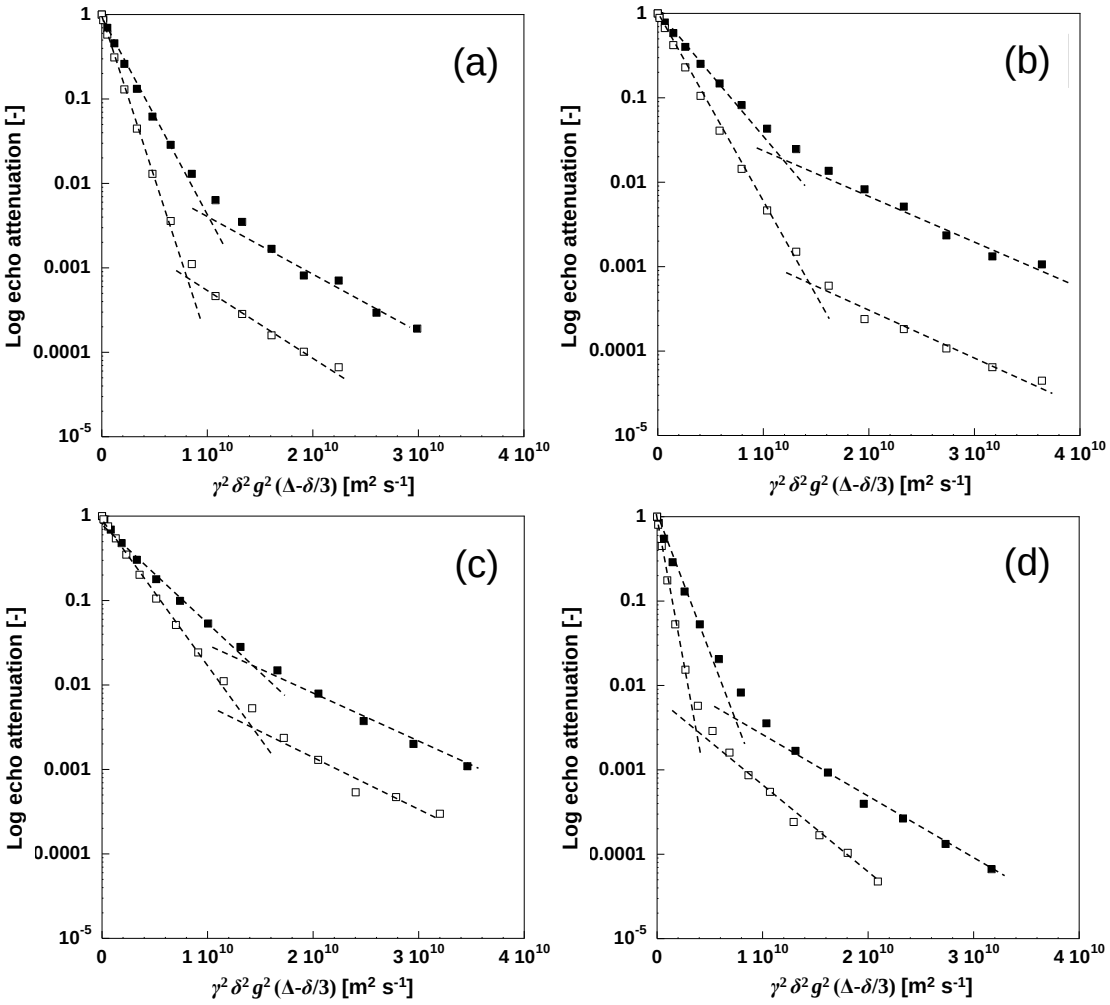

Figure 5. PFG-NMR echo attenuation plots for self-diffusion of guest molecules in MN 200 (closed symbols) and MN 500 (open symbols): (a) octane, (b) cyclohexane, (c) pyridine and (d) water. Dashed lines are fits using the bi-exponential form of Equation 1.

Table 7. Self-diffusion coefficients of the guest molecules in bulk liquid and in macropores and micropores of MN 200 and MN 500 at 20 ^{0}C. The method for estimating errors in the calculated values is shown in the Supplementary Information.

Guest molecule	D_0 (10^{-9} m^2/s)	D_1 (10^{-9} m^2/s)		D_2 (10^{-9} m^2/s)	
		MN 200	MN 500	MN 200	MN 500
cyclohexane	1.35 ± 0.03	0.40 ± 0.01	0.54 ± 0.01	0.09 ± 0.01	0.11 ± 0.01
n-octane	2.16 ± 0.04	0.63 ± 0.02	0.95 ± 0.02	0.15 ± 0.01	0.17 ± 0.01
pyridine	1.39 ± 0.03	0.39 ± 0.01	0.44 ± 0.01	0.09 ± 0.01	0.10 ± 0.01
water	2.05 ± 0.04	0.78 ± 0.02	1.71 ± 0.04	0.15 ± 0.01	0.22 ± 0.01

D_1 and D_2 represent self-diffusion coefficients of the guest molecules associated to the macroporous and microporous regions for the adsorbents, respectively.

The values of diffusivity in this study are in the range of 10^{-10}-10^{-9}m^2 s^{-1}, shown generally reductions greater than 50% relative to the bulk free liquid, which is typical of molecules confined in nanometre pores[35,36], agrees with the structural characteristics of the polymers used here. The average molecular displacement (RMSD = $\sqrt{2Dt}$ where the observation time t is 50 ms in the experiments) is of the order of 3-10 μm. This is much larger than the large polymer pore size (of the order nanometres) and implies that the probing molecules experienced many collisions with the pore walls, *i.e.,* we are in the range of tortuosity [35,48]. Hence, we can exclude that the fast component is the diffusion of the free liquid inside the large pores. The PFG parameters of the guest molecules in the two diffusion regimes of MN 200 and MN 500 are shown in Table 8. The tortuosity is a geometrical property of the pore network; hence, it is expected to be the same independently of the probe molecule used, assuming that changes in diffusion of such molecules will mostly be affected by geometrical features of the pore matrix rather than molecular interactions within the pore space, which is the case for hydrocarbons. The use of cyclohexane and n-octane as the probe molecules yields essentially similar values of PFG interaction parameters, the average value of which can be considered a good estimation of the tortuosity of the pore space [35], though they may refer to the

adsorbent tortuosities in the swollen state in contact with the liquid. A lower tortuosity of MN 500 relative to MN 200 can be observed, which could be due to the addition of sulfonic acid groups that may block some of the more tortuous diffusion pathways, leading to the formation of a less tortuous, connected (*i.e.,* percolation) pore network [49].

As the pores become smaller, the influence of the pore walls on diffusion of guest molecules will increase. When the pore size becomes comparable to the molecular diameter of the guest molecule, the obtained diffusivities tends to reflect pore wall effect [50], which is reflected in the high values for the PFG parameter in such small pores (ξ_2) , in addition to geometrical restrictions described by the tortuosity of the micropores.

Table 8. PFG parameters of guest molecules in macropores and micropores of MN 200 and MN 500 at 20 ^{0}C.

Guest molecule	MN 200		MN 500	
	ξ_1	ξ_2	ξ_1	ξ_2
cyclohexane	3.4 ± 0.1	15.0 ± 0.8	2.5 ± 0.1	12.9 ± 1.0
n-octane	3.4 ± 0.1	14.4 ± 1.5	2.3 ± 0.1	12.7 ± 0.8
pyridine	3.6 ± 0.1	15.4 ± 1.5	3.2 ± 0.1	13.9 ± 1.1
water	2.6 ± 0.1	13.4 ± 0.7	1.2 ± 0.1	9.3 ± 0.5

ξ_1 and ξ_2 represent PFG parameters of the guest molecules associated to the macroporous and microporous regions, respectively.

The behaviour of pyridine in MN200 is similar to that of the hydrocarbons, which implies that the reduction in diffusion rate of pyridine in the polymer is mainly affected by geometric features. In MN 500, the values of PFG interaction parameters for pyridine in both diffusion regions are greater than the tortuosity. This may be attributed to the presence of sulfonic acid groups in MN 500, which may induce changes in molecular interactions within the pore space, hence slowing down further the

diffusing species, which is in line with the finding that pyridine adsorption is faster on MN 500 in approaching equilibrium.

Water diffusion in both MN 500 and MN 200 shows an interesting behaviour. In MN 200, the PFG interaction parameters in both diffusion regions are approximately similar to values of tortuosity. However, in MN 500, the PFG interaction parameters in both diffusion regions, are significantly lower than the tortuosity. This behaviour of "enhanced" diffusivity could be attributed to a disruption of the hydrogen bonding network in the liquid by the interaction with the sulfonic acid groups, which has previously been observed for alcohols and polyols in porous materials [35,36].

The results show that PFG-NMR is able to give details of structural parameters such as pore network connectivity and its relation with the pore size distribution of the polymers adsorbents. In addition, they are able to elucidate the effect of molecular interactions within the pore space and the relationship with adsorption performances. The enhanced PFG parameter of pyridine on MN 500 further ties up the conclusion that the sulfonic acid functionalised MN 500 has better adsorption performances towards pyridine relative to MN200 from aqueous solutions.

The overall findings of PFG-NMR measurements give more insights into the physical and chemical behaviour of these systems and can be used for modelling purposes as well as aiding the selection of solvents, solute and polymers. Potential extension of this technique could be useful to study other effects in such processes, such as exploring the effect of pore size on the polymer performances as well as exploring their reusability and the effect of ageing on pore structure.

4. Conclusions

Hypercrosslinked polymeric adsorbents Macronet MN 200 and MN 500 were used to remove pyridine from aqueous solutions. Studies at variable solution pH revealed that pyridine uptake reaches an optimal uptake for both MN 200 and MN 500 as a result of optimal effect of π - π

hydrophobic and the attractive electrostatic interactions. The adsorption performance of MN 500 is greater than that of MN 200 and is less dependent on the solution pH.

The Langmuir maximum uptakes for the studied adsorbents in the adsorption isotherms were compared and showed superior pyridine uptake capacity compared to other types of porous materials reported in the literature. Langmuir equilibrium constants were used to evaluate the thermodynamic properties of pyridine uptake on MN 200 and MN 500 and showed the exothermic and endothermic natures of adsorption, respectively. Pyridine uptake on MN 500 proceeded faster than on MN 200. The adsorption kinetics was fitted to pseudo-first order and pseudo-second order rate models, revealing different pyridine adsorption mechanisms on MN 200 and MN 500, which is attributed to the presence of “reactive” sulfonic acid groups that functionalise the polymer surface in MN 500.

The effect of pore structure on diffusion and its link to adsorption performances were investigated using the PFG-NMR technique. The higher diffusion of pyridine in MN 500 can be linked to the faster kinetics observed for this polymer. The presence of two diffusion regions within the porous polymers can be observed, associated to the macroporous and microporous space, respectively, the latter influenced by pore wall effects on diffusion of guest molecules. The higher PFG interaction parameter, relatively to the tortuosity, of pyridine on MN 500 can be explained by the presence of sulfonic acid groups on MN 500, which can be linked to the higher adsorption performance of this polymer.

In conclusion, we have characterised and shown with a series of techniques, including PFG-NMR studies, that Macronet polymers and particularly the MN 500 type are potentially very attractive adsorbents in waste water treatment with pyridine and its derivatives as contaminants.

Acknowledgements

Carmine D'Agostino would like to acknowledge Wolfson College, Cambridge, for supporting his research activities.

5. References

[1] M. Feldmannova, K. Hilscherova, B. Marsalek, L. Blaha, Effects of N-heterocyclic polyaromatic hydrocarbons on survival, reproduction, and biochemical parameters in daphnia magna, Environ. Toxicol. 21 (2006) 425–431.

[2] K.V. Padoley, S.N. Mudliar, R.A. Pandey, Heterocyclic nitrogenous pollutants in the environment and their treatment options--an overview, Bioresour. Technol. 99 (2008) 4029–4043.

[3] G.K. Sims, E.J. O'Loughlin, R.L. Crawford, Degradation of pyridines in the environment, Crit. Rev. Environ. Control. 19 (1989) 309–340.

[4] D. Mohan, K.P. Singh, S. Sinha, D. Gosh, Removal of pyridine from aqueous solution using low cost activated carbons derived from agricultural waste materials, Carbon N. Y. 42 (2004) 2409–2421.

[5] B.H. Hameed, D.K. Mahmoud, A.L. Ahmad, Equilibrium modeling and kinetic studies on the adsorption of basic dye by a low-cost adsorbent: coconut (cocos nucifera) bunch waste, J. Hazard. Mater. 158 (2008) 65–72.

[6] D.H. Lataye, I.M. Mishra, I.D. Mall, Pyridine sorption from aqueous solution by rice husk ash (RHA) and granular activated carbon (GAC): parametric, kinetic, equilibrium and thermodynamic aspects, J. Hazard. Mater. 154 (2008) 858–870.

[7] J.-H. Tsai, H.-M. Chiang, G.-Y. Huang, H.-L. Chiang, Adsorption characteristics of acetone, chloroform and acetonitrile on sludge-derived adsorbent, commercial granular activated carbon and activated carbon fibers, J. Hazard. Mater. 154 (2008) 1183–91.

[8] C.-F. Chang, C.-Y. Chang, K.-E. Hsu, S.-C. Lee, W. Höll, Adsorptive removal of the pesticide methomyl using hypercrosslinked polymers, J. Hazard. Mater. 155 (2008) 295–304.

[9] X. Zeng, T. Yu, P. Wang, R. Yuan, Q. Wen, Y. Fan, C. Wang, R. Shi, Preparation and characterization of polar polymeric adsorbents with high surface area for the removal of phenol from water, J. Hazard. Mater. 177 (2010) 773–780.

[10] C. Valderrama, J.L. Cortina, A. Farran, X. Gamisans, C. Lao, Kinetics of sorption of polyaromatic hydrocarbons onto granular activated carbon and Macronet hyper-cross-linked polymers (MN200), J. Colloid Interface Sci. 310 (2007) 35–46.

[11] C. Valderrama, X. Gamisans, X. de las Heras, A. Farran, J.L. Cortina, Sorption kinetics of polycyclic aromatic hydrocarbons removal using granular activated carbon: intraparticle diffusion coefficients, J. Hazard. Mater. 157 (2008) 386–396.

[12] H. Zhang, A. Li, J. Sun, P. Li, Adsorption of amphoteric aromatic compounds by hyper-cross-linked resins with amino groups and sulfonic groups, Chem. Eng. J. 217 (2013) 354–362.

[13] C. Valderrama, J.I. Barios, M. Caetano, A. Farran, J.L. Cortina, Kinetic evaluation of phenol/aniline mixtures adsorption from aqueous solutions onto activated carbon and hypercrosslinked polymeric resin (MN200), React. Funct. Polym. 70 (2010) 142–150.

[14] C. Valderrama, J.L. Cortina, A. Farran, X. Gamisans, F.X. de las Heras, Evaluation of hyper-cross-linked polymeric sorbents (Macronet MN200 and MN300) on dye (Acid red 14) removal process, React. Funct. Polym. 68 (2008) 679–691.

[15] L.J. Abbott, C.M. Colina, Formation of Microporosity in Hyper-Cross-Linked Polymers, Macromolecules. 47 (2014) 5409–5415.

[16] C. Valderrama, J.L. Cortina, A. Farran, X. Gamisans, F.X. de las Heras, Kinetic study of acid red “dye” removal by activated carbon and hyper-cross-linked polymeric sorbents Macronet Hypersol MN200 and MN300, React. Funct. Polym. 68 (2008) 718–731.

[17] J.E. Tanner, Use of the stimulated echo in NMR diffusion studies, J. Chem. Phys. 52 (1970) 2523–2526.

[18] R.M. Cotts, M.J.R. Hdch, T. Sun, J.T.I. Markert, Pulsed field gradient stimulated echo methods for improved NMR diffusion measurements in heterogeneous systems, J. Magn. Reson. 266 (1989) 252–266

[19] D.S. Stefan, I. Pincovschi, Adsorption of phenol and its chlorinated derivatives from waste waters using hypercrosslinked polymers, Rev. Chim. 64 (2013) 1381–1384.

[20] C.M. Bohdana, S.D. Cantea, E. Pincovichi, A.-M. Oancea, Proton/magnesium (II) ion exchange equilibrium on sulfonated hyper-crosslinked resin, Rev. Chim. 62 (2011) 233–239.

[21] D. Kaušpėdienė, E. Kazlauskienė, R. Česūnienė, A. Gefenienė, R. Ragauskas, A. Selskienė, Removal of the phthalocyanine dye from acidic solutions using resins with the polystyrene divinylbenzene matrix, Chemija. 24 (2013) 171–181.

[22] W. Yang, Y. Lu, F. Zheng, X. Xue, N. Li, D. Liu, Adsorption behavior and mechanisms of norfloxacin onto porous resins and carbon nanotube, Chem. Eng. J. 179 (2012) 112–118.

[23] E. Karounou, Removal of endocrine disruptors by activated carbons and hypercrosslinked polymeric adsorbents, PhD thesis, Loughborough University 2004.

[24] H. Bouyarmane, S. El Asri, A. Rami, C. Roux, M.A. Mahly, A. Saoiabi, et al., Pyridine and phenol removal using natural and synthetic apatites as low cost sorbents: influence of porosity and surface interactions, J. Hazard. Mater. 181 (2010) 736–741.

[25] F. Liu, J. Zhao, S. Wang, P. Du, B. Xing, Effects of solution chemistry on adsorption of selected pharmaceuticals and personal care products (PPCPs) by graphenes and carbon nanotubes, Environ. Sci. Technol. 48 (2014) 13197–13206.

[26] P. Alonso-Davila, O.L. Torres-Rivera, R. Leyva-Ramos, R. Ocampo-Perez, Removal of pyridine from aqueous solution by adsorption on an activated carbon cloth, Clean - Soil, Air, Water. 40 (2012) 45–53.

[27] K.Y. Foo, B.H. Hameed, Insights into the modeling of adsorption isotherm systems, Chem. Eng. J. 156 (2010) 2–10.

[28] M.M. Broholm, K. Broholm, E. Arvin, Sorption of heterocyclic compounds on natural clayey till, J. Contam. Hydrol. 39 (1999) 183–200.

[29] Y. Zhang, D. Li, Adsorption of pyridine on post-crosslinked fiber, J. Sci. Ind. Res. 69 (2010) 73–

76.

[30] P. Liao, S. Yuan, W. Xie, W. Zhang, M. Tong, K. Wang, Adsorption of nitrogen-heterocyclic compounds on bamboo charcoal: kinetics, thermodynamics, and microwave regeneration, J. Colloid Interface Sci. 390 (2013) 189–195.

[31] N.A. Oladoja, C.O. Aboluwoye, Y.B. Oladimeji, Kinetics and isotherm studies on methylene blue adsorption onto ground palm kernel coat, Turkish J. Eng. Env. Sci. 32 (2008) 303–312.

[32] G. Alberti, V. Amendola, M. Pesavento, R. Biesuz, Beyond the synthesis of novel solid phases: Review on modelling of sorption phenomena, Coord. Chem. Rev. 256 (2012) 28–45.

[33] Y.S. Ho, G. Mckay, A comparison of chemisorption kinetic models applied to pollutant removal on various sorbents, Process Saf. Environ. Prot. 76 (1998) 332–340.

[34] Y.S. Ho, G. Mckay, Sorption of dye from aqueous solution by peat, Chem. Eng. J. 70 (1998) 115–124.

[35] M.D. Mantle, D.I. Enache, E. Nowicka, S.P. Davies, J.K. Edwards, C.D. Agostino, D.P. Mascarenhas, L. Durham, M. Sankar, D.W. Knight, L.F. Gladden, S.H. Taylor, G.J. Hutchings, Pulsed-field gradient NMR spectroscopic studies of alcohols in supported gold catalysts, J. Chem. Phys. C (2011) 1073–1079.

[36] C. D'Agostino, J. Mitchell, L.F. Gladden, M.D. Mantle, Hydrogen bonding network disruption in mesoporous catalyst supports probed by PFG-NMR diffusometry and NMR relaxometry, J. Phys. Chem. C. 116 (2012) 8975–8982.

[37] S. Vasenkov, P. Kortunov, PFG NMR measurements of tortuosity factors for diffusion in meso- and macropores of FCC catalysts, Diffus. Fundam. 1 (2005) 2.1–2.11.

[38] C. D'Agostino, T. Kotionova, J. Mitchell, P.J. Miedziak, D.W. Knight, S.H. Taylor, G.J. Hutchings, L.F. Gladden, M.D. Mantle, Solvent effect and reactivity trend in the aerobic oxidation of and relaxation studies, Chem. A Eur. J. 19 (2013) 11725–11732.

[39] C. D'Agostino, G.L. Brett, P.J. Miedziak, D.W. Knight, G.J. Hutchings, L.F. Gladden, M.D. Mantle, Understanding the solvent effect on the catalytic oxidation of 1,4-butanediol in methanol over Au/TiO2 Catalyst: NMR diffusion and relaxation Studies, Chem. Eur. J. 18 (2012) 14426–14433.

[

[40] M.P. Hollewand, L.F. Gladden, Transport heterogeneity in porous pellets-I. PGSE NMR studies,

Chem. Eng. Sci. 50 (1995) 309–326.

[41] N.A. Penner, P.N. Nesterenko, M.M. Ilyin, M.P. Tsyurupa, V.A. Davankov, Investigation of the properties of hypercrosslinked polystyrene as a stationary phase for high-performance liquid chromatography, Chromatographia 50 (1999) 611-620.

[42] M.P. Tsyurupa, Z.K. Blinnikova, N.A. Proskurina, A.V. Pastukhov, L.A. Pavlova, V.A. Davankov, Hypercrosslinked polystyrene: The first nanoporous polymeric material, Nanotechnologies Russ. 4 (2009) 665–675.

[45] C. D'Agostino, Y. Ryabenkova, P.J. Miedziak, S.H. Taylor, G.J. Hutchings, L.F. Gladden, M.D. Mantle, Deactivation studies of a carbon supported AuPt nanoparticulate catalyst in the liquid-phase aerobic oxidation of 1,2-prooanediol, Catal. Sci. Technol. 4 (2014) 1313–1322.

[44] W. Brown, P. Stilbs, T. Lindstrom, Self-diffusion of small molecules in cellulose gels using FT-pulsed field gradient NMR, J. Appl. Polym. Sci. 29 (1984) 823–827.

[45] S. Hurrell, R.E. Cameron, Polyglycolide: Degradation and drug release. Part I: Changes in morphology during degradation, J. Mater. Sci. Mater. Med. 12 (2001) 811–816.

[46] G.E. Milroy, R.E. Cameron, M.D. Mantle, L.F. Gladden, H. Huatan, The distribution of water in degrading polyglycolide. Part II: Magnetic resonance imaging and drug release, J. Mater. Sci. Mater. Med. 14 (2003) 465–473.

[47] J.G. Seland, M. Ottaviani, B. Hafskjold, A PFG-NMR study of restricted diffusion in heterogeneous polymer particles, J. Colloid Interface Sci. 239 (2001) 168–177.

[48] P.T. Callaghan, Principles of nuclear magnetic resonance microscopy. Oxford University Press, Oxford, 1993.

[49] P. Kortunov, S. Vasenkov, J. Kärger, R. Valiullin, P. Gottschalk, M. Fé Elía, M. Perez, M. Stöcker, B. Drescher, G. McElhiney, C. Berger, R. Gläser, J. Weitkamp, The role of mesopores in intracrystalline transport in USY zeolite: PFG NMR diffusion study on various length scales, J. Am. Chem. Soc. 127 (2005) 13055–13059.

[50] F. Stallmach, J. Kärger, The potentials of pulsed field gradient NMR for investigation of porous media, Adsorption. 133 (1999) 117–133.